

New Method for Synthesis of Zinc Metaborate $Zn_4B_6O_{13}$ Crystals via Sol-Gel Process and Investigation of DFT Calculations

Abdolali Alemi^{1*}, Nasrin Mohseni¹, Mahboubeh Dolatyari², Akbar Bakhtiari¹

¹ *Department of Inorganic Chemistry, Faculty of Chemistry, University of Tabriz, Tabriz, Iran*

² *Laboratory of Photonics & Nano Crystals, School of engineering-Emerging Technologies, University of Tabriz, Tabriz, Iran*

Received: 18 February 2012; Accepted: 23 April 2012

ABSTRACT

In this work facile sol-gel (pechni) method has been successfully established to synthesize $Zn_4B_6O_{13}$ nanocrystals which have cubic crystals with lattice parameter: $a = 7.48 \text{ \AA}$. The structure and morphology of the obtained material were studied by X-ray diffraction (XRD), Infrared spectra (IR), scanning electron microscopy (SEM) and photoluminescence analysis. The experimental results show a band gap of 3.306 eV for the synthesized materials. Density functional theory (DFT) calculations by GGA-PBE method show, the crystals belong to the semiconductors with an indirect energy band gap of about 3.289 eV. The calculated band gap using the GGA-PBE method is comparable with the experimental results. The optical properties include the dielectric spectra; absorption, reflectivity and energy-loss spectra, and the origin of spectral peaks were analyzed based on the electronic structures.

Keyword: Zinc metaborate; nanocrystals, Sol-Gel; Photoluminescence, DFT calculations.

1. INTRODUCTION

Inorganic borates have attracted considerable attention in the past decades due to their important practical applications as second harmonic generation optical materials, host material for fluorescence, piezoelectric and ferroelectric materials to semiconducting behaviour [1,2]. They are recognized as expensive, easily applicable, flame retardant and more importantly environ-

mentally safe preservative [3]. In the borate systems a boron atom may adopt triangular (BO_3) or tetrahedral (BO_4) oxygen coordination.

The BO_3 and BO_4 group may be further linked via common oxygen atoms to form isolated rings and cages or polymerize in to infinite chains, sheets and networks, leading to the rich structural chemistry [2].

(*) Corresponding Author - e-mail: alemi@tabrizu.ac.ir

As borate salts, zinc borates have been the subject of significant research for applications including a polymer additive which serves as a fire retardant synergists, char promoter, anti-arcing agent, a preservative in wood composites, smoke and afterglow suppressant additive, wear resistance and optical properties [4]. In the binary systems of ZnO-B₂O₃, at least three compounds have been proposed including ZnB₄O₇ (zinc tetraborate), Zn₃B₂O₆ (zinc orthoborate), and Zn₄O (BO₂)₆ (zinc metaborate) [5]. Among them zinc metaborate cubic crystals were obtained by thermal treatment from melts of ZnO: B₂O₃ for the first time and fluorescent data were reported [6]. Then single crystal of this composition was provided by professor J. Liebertz (in 1982) through the czocralsky method, and their photoluminescence, thermo-luminescence and EPR properties was studied (in 1990) [7].

In the last decade, several low temperature preparation techniques have been used to prepare fine particle systems such as co- precipitation, sol-gel method and hydrothermal synthesis.

Despite of some significant experimental achievements, our knowledge on their structural, electrical and optical properties, which would be of primary importance for the applications, is still rather limited. Therefore, further theoretical investigations concerning their microscopic properties are very necessary. Recent advances in the computer performance and computer codes makes it possible to study the chemical nature of condensed materials, such as metal, alloy, ceramics and others, by *ab initio* calculation that is a powerful tool to know how the electrons affect the property of substance.

In this research work Zn₄B₆O₁₃ nanocrystals was prepared by pechini method. This technique known due to the low cost and versatility is a low temperature synthetic method that uses the dissolution of cations in an aqueous citric acid (CA) solution. Ethylene glycol (EG) addition promotes polymerization (esterification). After polymerization the segregation of cations during thermal decomposition is minimal, owing to the formation of high viscosity polyester. Also, we will present a

systematic study of the electronic and optical properties of the synthesized materials through the density functional theory calculations.

2. EXPERIMENTAL

2.1. Synthesis

In the preparation of Zn₄B₆O₁₃, Zn (NO₃)₂.6H₂O and H₃BO₃ precursors were dissolved in deionized water in molar ratio 1:4 (excess of H₃BO₃ was added to compensate for B₂O₃ evaporation). The solution was heated at 70°C, then citric acid (CA) in molar ratio of 3:1 (CA: Zn²⁺) and ethylene glycol (EG) in weight ratio of 3.6:1 (CA: EG) was added under stirring and the mixture was heated at 90°C. So formation of brown transparent glassy polymeric resin with enormous swelling was observed. The obtained resin was heated at 350°C for 3h resulting in a fluffy black mass, which was grounded into a powder. Finally this material was calcinated at different temperatures and times and the optimized condition was obtained by heating at 850°C during 3h.

2.2. Characterization

X-ray powder diffraction (XRD) was performed with a Siemens D5000 X-ray diffractometry with Cu-k_α line of wavelength λ=1.541Å at the scanning rate of 2°/min and 2θ was varied from 4° to 70°. The morphology of particles was studied by Scanning Electron Microscope (SEM, Stereo scan s 360 microscope). The FT-IR transmission spectra in the region 400-4000 cm⁻¹ were recorded for all the samples using FT-IR Nexus 670 by KBr pellet technique. The photoluminescence (PL) excitation and emission spectra were taken on a Perkin Elmer spectrofluorimeter.

3. RESULTS AND DISCUSSION

3.1. Powder X-ray diffraction studies

Phase identification and crystallinity of the synthesized materials examined by Powder x-ray diffraction. Figure 1 shows a typical P-XRD pattern

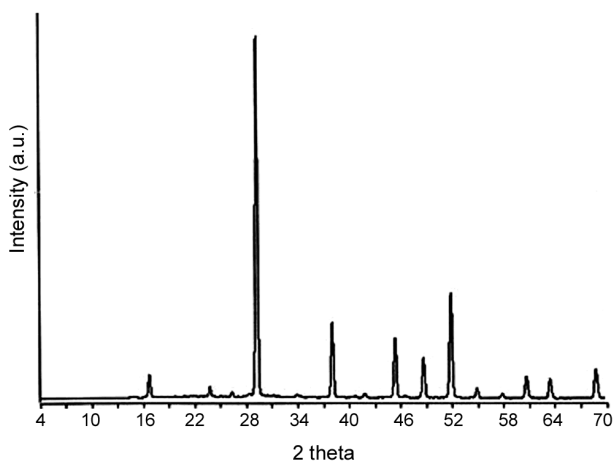


Figure 1: XRD pattern of the synthesized $Zn_4B_6O_{13}$ via sol-gel method at $850^\circ C$ for 3h.

of the synthesized $Zn_4B_6O_{13}$ in optimized conditions. All diffraction peaks were quite similar to those of bulk $Zn_4B_6O_{13}$ and diffraction data were in good agreement with ASTM standard (ASTM 21-1469) and earlier reports [8, 9].

No characteristic peaks of impurities such as $Zn_3B_2O_6$, ZnB_4O_7 , other zinc borates, unreacted compound and so on were observed.

P-XRD patterns of the materials at different calcinations temperatures are presented in Figure 2.

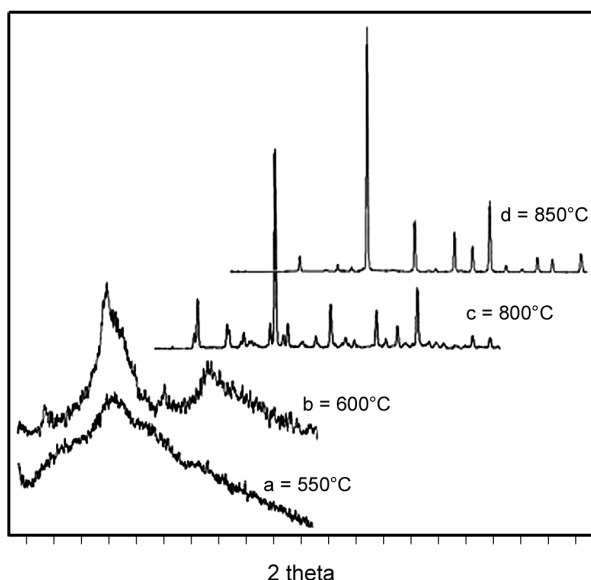


Figure 2: XRD patterns of the obtained $Zn_4B_6O_{13}$ via sol-gel method at different temperatures.

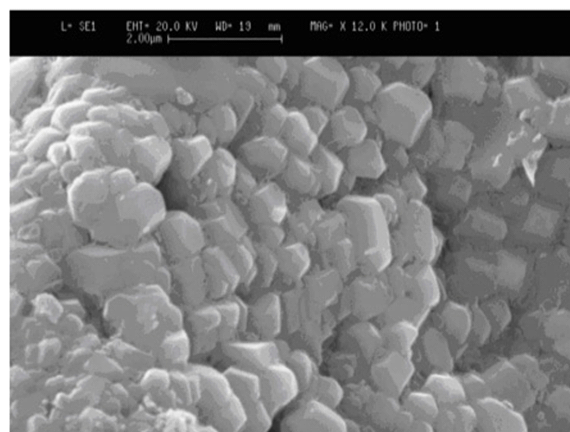


Figure 3: SEM images of zinc metaborate sample synthesized by sol-gel method.

Samples obtained at $550^\circ C$ and $600^\circ C$ are amorphous phases. A crystalline phase of $Zn_4B_6O_{13}$ grows by increasing the temperature. Cubic crystals of $Zn_4B_6O_{13}$ were obtained at $800^\circ C$ accompany with minor impurities, which were eliminated by crystallizing at $850^\circ C$.

The cell parameter of $Zn_4B_6O_{13}$ was determined by CELREF version 3 software, using of XRD data. The results indicate, the obtained metaborate can be indexed on the base of cubic with lattice parameter $a = 4.48 \text{ \AA}$.

3.2. Morphology

Figure 3 shows a typical scanning electron microscope (SEM) image of the zinc metaborate sample prepared from sol-gel method at $850^\circ C$. It can be seen that the particles have cubic like morphology with the particle size in the range 400-600 nm.

3.3. Infrared spectra studies

Figure 4 shows the FT-IR spectra of the obtained materials at different temperatures. At lower calcination temperature ($550^\circ C$) absorption peaks between 1250 and 1500 cm^{-1} are those of typical for triangular borate group (BO_3) as in $LaBO_3$ [4]. However, in higher calcination temperatures ($700^\circ C$ - $850^\circ C$), strong absorption peaks observed between 600 to 1100 cm^{-1} (714.54 , 926.70 , 953.450 and 1086.86 cm^{-1}) are normally typical for tetra-

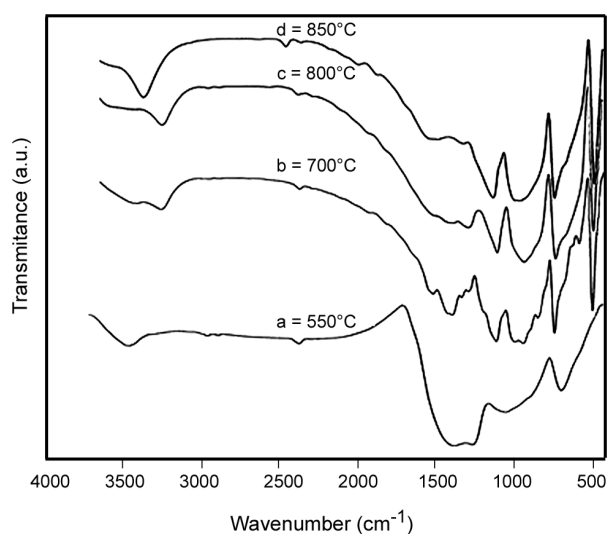


Figure 4: FT-IR spectra of synthesized materials at different final temperatures.

hedral borate groups (BO_4) [2, 10-12]. According to these results at low calcination temperatures, BO_3 groups are formed, which led to a transformation to the BO_4 groups by heating at high temperatures. Also the presence of the absorption band at 472 cm^{-1} is related to the Zn-O vibration [13].

3.4. Luminescent properties

The practical phosphors were focused mainly on some oxygen containing inorganic compounds, such as oxides, aluminates and borates. They usually have suitable host absorption band, which can be used by luminescent center. The emission spectrum of $\text{Zn}_4\text{B}_6\text{O}_{13}$ particles prepared by sol-gel method is shown in Figure 5. Upon UV irradiation, the $\text{Zn}_4\text{B}_6\text{O}_{13}$ crystals show a violet emission with strong afterglow. This emission consists of a broad band with maximums at 428 and 490 nm. There are the shoulders at 375, 398, 450 and 520 nm too. This spectrum is similar to which obtained by Meijerinc and his co-workers for this material [7]. The emission spectrum of the obtained material shows that the first band in the nano scale sample has shifted to short wavelength compared to the bulk sample synthesized by Meijerinc groups. (This peak in bulk sample has observed at 440 nm) [7]. According to this spectrum the band gap energy of

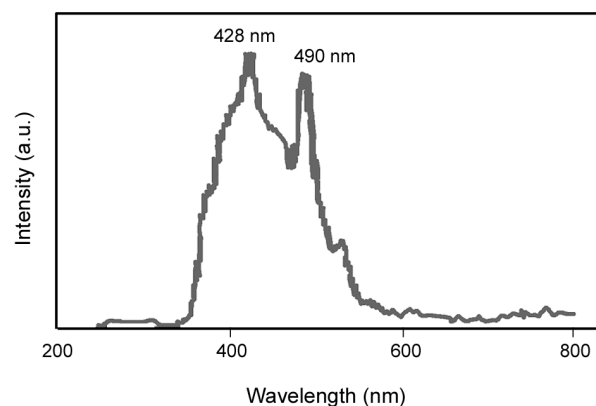


Figure 5: Emission spectrum of synthesized $\text{Zn}_4\text{B}_6\text{O}_{13}$ crystals.

synthesized $\text{Zn}_4\text{B}_6\text{O}_{13}$ crystal is 3.306 eV that increases with decreasing of particle size [14].

The calculated band structure of the compound along high symmetry points of the first Brillouin zone is plotted in Figure 6, where the labeled k points are present as G (0.000, 0.000, 0.000), H (0.500, -0.500, 0.500), N (0.000, 0.000, 0.500), P (0.250, 0.250, 0.250). It is found that the top of the valence bands (VBs) has a small dispersion, whereas the bottom of the conduction bands (CBs) has a big dispersion. The lowest energy (3.289 eV) of conduction bands (CBs) is localized at the G point, and the highest energy (0.00 eV) of VBs is localized at the N point. According to our calculations, the value of calculated band gap for this material is 3.289 eV which is comparable with the experimental values measured from photo luminescence spectrum.

Total density of states (TDOS), along with Zn 3s, 3p, 3d, B 2s, 2p, O-2s, 2p and partial densities

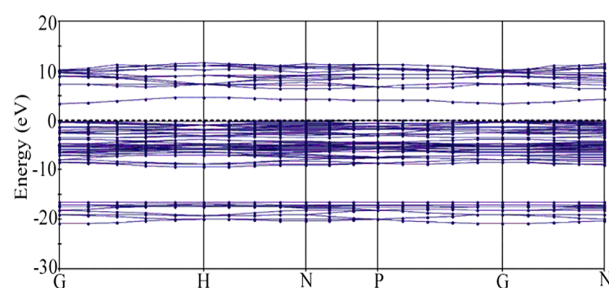


Figure 6: Band structure of $\text{Zn}_4\text{B}_6\text{O}_{13}$.

of states (PDOS) for $Zn_4B_6O_{13}$ crystals are shown in Figure 7.

According to the band structure and the density of states (DOS), the energy bands can be divided into three groups. The lowest group has significant

contributions from O-2s states at -21.11 eV to -15.83 eV. However, contributions from B-2s, 2p and small admixture from Zn-2s, -2p states still can be observed at these energy intervals. The most complex bands denoted as valence bands are from

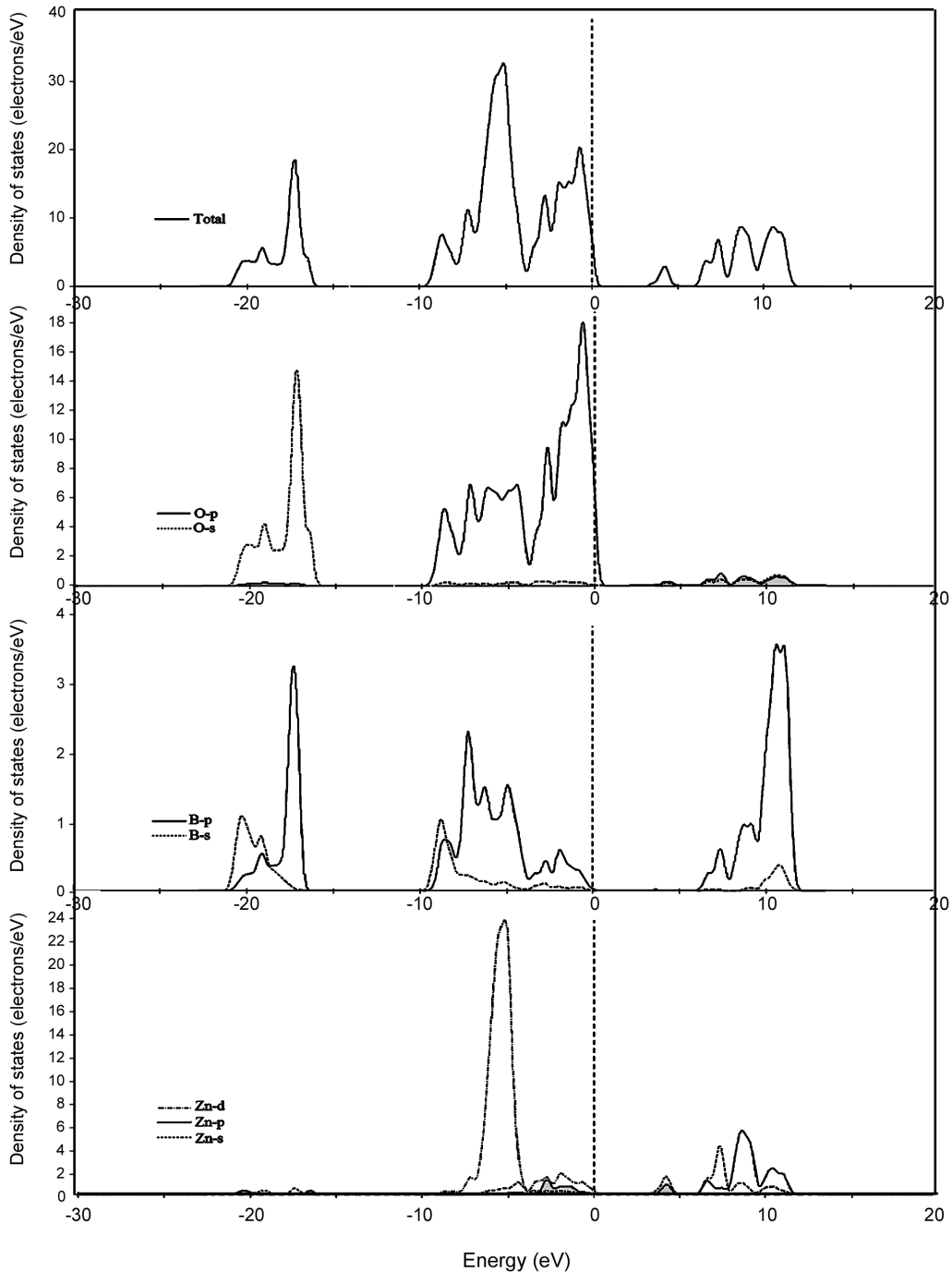


Figure 7: Total and partial densities of states for zinc metaborate. The position of the Fermi level is set at 0 eV.

-9.72 eV to the Fermi level (0.0 eV). According to the partial density of states, it can be confirmed that the valence bands are mainly composed by O-2p, along with small admixture Zn-3s, 3p and B-2s, 2p while the contributions from Zn-3d states are significant and cannot be neglected. Moreover, it can be observed that the energy bands from -9.72 eV to the Fermi level can be further divided into three parts. Such a splitting characteristic of valence bands reflects different bonding behaviors. The first parts located at -9.72 eV to -7.56 eV is due to the weak interaction between O-2p, B-2s, 2p orbits while the second part from -7.56 eV to -3.59 eV indicates the covalent bonds between Zn-3d and O-2p orbits. The third part from 3.59 to the Fermi level indicates the weak bonding between Zn-3p, 3d, B- 2p orbits and O-2p orbits. The PDOS in Figure 7 also suggest hybridization between B-2s, 2p orbits, Zn-3s-3p-3d and O-2s, 2p orbits. The conduction bands from 2.89 eV to 11.45 eV come from Zn-3s, 3p states and B-2s, 2p states and O-3s, 3p states.

The optical properties of a solid material are usually described by the complex dielectric function $\epsilon(\omega) = \epsilon_1(\omega) + i\epsilon_2(\omega)$, which characterizes the linear response of the material to an electromagnetic radiation, and therefore governs the propagation behavior of radiation in a medium. The imaginary part of the dielectric function $\epsilon_2(\omega)$ represents the optical absorption in the crystal, which can be calculated from the momentum matrix elements between the occupied and unoccupied states, and the real part $\epsilon_1(\omega)$ is evaluated from the imaginary part $\epsilon_2(\omega)$ by the Kramers-Kronig transformation.

Based on the electronic structure, the dielectric functions of $Zn_4B_6O_{13}$ were calculated. The $\epsilon_1(\omega)$

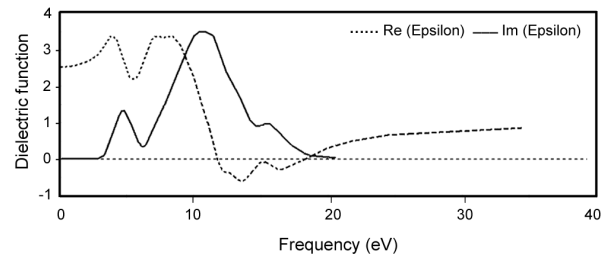


Figure 8: Dielectric functions of $Zn_4B_6O_{13}$.

and $\epsilon_2(\omega)$ as a function of the photon energy are shown in Figure 8.

It can be seen that imaginary part of $\epsilon(\omega)$ in Zinc Metaborate have three bands located at 4.96 eV, 10.75 eV, 15.50 eV with a shoulder at 13 eV. The first Peak located at 4.96 eV is corresponds mainly to the transition from O-2p VB to the empty Zn-3s, 3p. The peak at 10.75 eV is related to O-2p VB to the empty B-2p and Zn-2s, 2p. The shoulder at 13 eV and the peak located at 15.50 eV could be related to O-2p VB to the empty B-2p and Zn-2s, 2p. It is noted that a peak in $\epsilon_2(\omega)$ does not correspond to a single interband transition since many direct or indirect transitions may be found in the band structure with an energy corresponding to the same peak [15]. For the real part $\epsilon_1(\omega)$ of the dielectric function $\epsilon(\omega)$, the most important quantity is the zero frequency limit $\epsilon_1(0)$ which is the electronic part of the static dielectric constant that depends strongly on the band gap. We note that a smaller energy gap yields a larger $\epsilon_1(0)$ value. This could be explained on the basis of the Penn model ($\epsilon_1(0) \approx 1 + (\hbar \omega_p / E_g)^2$) [16]. We can determine E_g from this expression by using the values of $\epsilon_1(0)$ and the plasma energy $\hbar \omega_p$. The calculated static dielectric constants $\epsilon_1(0)$ are listed in Table 1. The calculated results on the

Table1: Theoretical and experimental lattice constants (a, b, c), energy gaps E_g and the average static dielectric constant of $Zn_4B_6O_{13}$.

		Pseudopotentials	a (Å)	E_g (eV)	$\epsilon_1(0)$
$Zn_4B_6O_{13}$	Calculation	Norm-conserving	7.33	3.289	3.5
	Experimental		7.48	3.306	

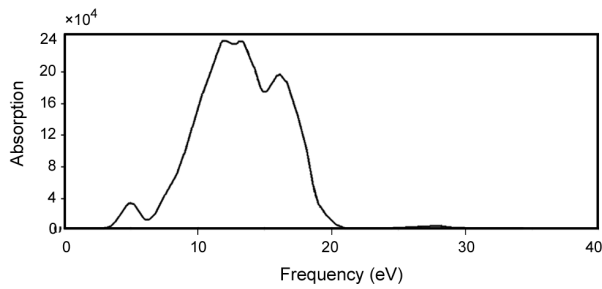


Figure 9: Calculated absorption spectra of $Zn_4B_6O_{13}$.

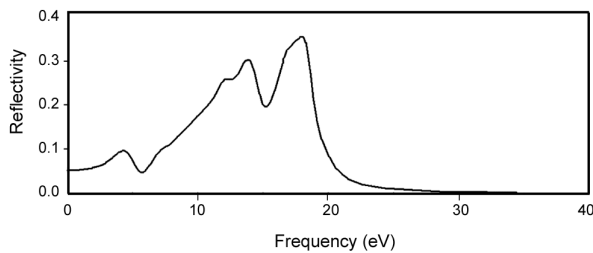


Figure 10: Calculated reflectivity of $Zn_4B_6O_{13}$.

absorption, reflectivity and energy-loss spectra by NCP (Norm-Conserving Pseudopotentials) were shown in Figures 9-11. According to the absorption spectra, the absorption edges are located at 5 eV, 11.91 eV, 13.24 eV, and 16.06 eV. The absorption coefficients decrease rapidly in the low-energy region, which is the representative character of the semiconductor and insulator. In the range from 0 to 5 eV the reflectivity was lower than 10 %. The calculated reflectivity has a maximum value of roughly 35.0% at about 18 eV. From the absorption and reflectivity spectra, we can conclude that this material is transmitting for frequencies <1.89 eV. The energy-loss spectrum describes the energy-loss of a fast electron traversing in the material [17]. The

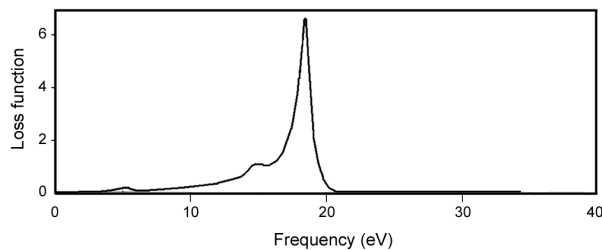


Figure 11: Calculated Energy loss function for $Zn_4B_6O_{13}$.

main peak is generally defined as the bulk plasma frequency [18]. According to Figure 11, the main peak of energy-loss spectra is at about 18.5 eV. Such calculations may stimulate the experimental investigations.

4. CONCIOUSIONS

In summary, Zinc metaborate nanocrystals were successfully synthesized by $Zn(NO_3)_2 \cdot 6H_2O$ and H_3BO_3 as a raw materials and citric acid (CA), ethylene glycol (EG) as esterification or gelling agents through pechini method, under heating at $850^\circ C$ during 3h. Powder x-ray diffraction analysis confirmed synthesis of high crystalline $Zn_4B_6O_{13}$. FT-IR analysis confirms the existence of BO_4 groups. SEM analysis indicates that the morphology of product displays cubic like morphology with average size of 400-600 nm. Also, the PL spectrum shows a band gap of 3.306eV for obtained material.

Also, this research work reports study of the structural, electronic and optical properties of zinc metaborate using the density functional theory within the generalized gradient approximation. The results for band structure and density of states show that this material has an indirect energy band gap of about 3.289eV. The optical properties, including the dielectric function, absorption coefficient, reflectivity and energy-loss spectra, also have been presented. According to the absorption and reflectivity spectra, zinc metaborate is theoretically transmitting for frequencies <1.89 eV. Furthermore, the imaginary part $\epsilon_2(\omega)$ of the dielectric function $\epsilon(\omega)$ has been discussed in detail according to the band structure.

ACKNOWLEDGEMENTS

This study has been supported by the council of university of Tabriz. The authors thank the material and energy center of karaj for SEM images, and Miss. Roghaye Ebrahimi Kalan for her cooperation.

REFERENCES

1. Chen D.G., Cheng W.D., Wu D.S., Zhang H., Zhang Y.C., Gong Y.J. and Kan Z.G., *Solid state Sci.*, **7**(2005), 179.
2. Xuean C.X., Zhao Y., Chang X., Zuo J., Zang H. and Xiao W., *J. Solid State Chem.*, **179**(2006), 3911.
3. Baysal E., Sonmez A., Colak M. and Toker H., *Bioresource Technol.*, **97**(2006), 2271.
4. Tian Y., Guo Y., Jiang M., Sheng Y., Hari B., Zhang G., Jiang Y., Zhou B., Zhu Y. and Wang Z., *Mater. Lett.*, **60**(2006), 2511.
5. Chen X., Xue H., Chang X., Zhang L., Zhao Y., Zuo J., Zang H. and Xiao W., *J. Alloys Compd.*, **425**(2006), 96.
6. Terol S. and Otero M.J., *Z. Naturforsch.*, **16a** (1967), 920.
7. Meijerink A., Blasse G. and Glasbeek M., *J. Phys.: Condens. Matter*, **2**(1990), 6303.
8. Shulan C., Shanlan L., Yuhe K. and Sihong W., *J. Rare Earth*, **20**(2002), 606.
9. Papazoglou P., Eleftheriou E., Zaspalis V.T. and Magn J., *Magn. Mater.*, **296**(2006), 25.
10. Hupperz H. and Heymann G., *Solid State Sci.*, **5**(2003), 281.
11. Stefani R., Maia A.D., Teotonio E.E.S., Monteiro M.A.F., Felinto M.C.F.C. and Brito H.F., *J. Solid State Chem.*, **179**(2006), 1089.
12. Heymann G., Sotner T. and Huppertz H., *Solid State Sci.*, **8**(2006), 21.
13. Shan G., Xiao X., Wang X., Kong X. and Liu Y., *J. Colloid. Interf. Sci.*, **298**(2006), 172.
14. Colmenares J.C., Aramendia M.A., Marinas A., Marinas J.M. and Urbano F.J., *Appl. Catal. A-Gen.*, **306**(2006), 120.
15. Paszkowicz W., Wolska A., Klepka M.T., All S.A.E. and Eldin F.M.E., *Acta Physica Polonica A*, **117**(2010), 315.
16. Hesse K.F., *Acta Cryst. B*, **33**(1977), 901.
17. Smith R.I., Howie R.A., West A.R. and Pina A.A., *Acta Crystallographica, Section C*, **46**(1990), 363.
18. Tang T. and Luo D.L., *J. At. Mol. Sci.*, **1**(2010), 185.